High Quantum Efficiency SWIR Sensor Using Digital Alloy

Balasekaran SUNDARARAJAN*, Makoto MURATA, and Yasuhiro IGUCHI

A SWIR sensor which operates in the wavelength region from 1 to 2.5 μm is expected to be applied in a variety of fields such as agriculture, medical diagnostics, industrial inspection, space observation, etc. We have developed SWIR sensors with the cut-off wavelength of 2.5 μm and low dark current by using InGaAs/GaAsSb quantum well structures as the light-receiving layer. The theoretical calculation of quantum well structure indicated improvement of quantum efficiency by replacing InGaAs of this quantum well with digital alloy consisting of InAs and GaAs. This paper describes the performance of SWIR sensor with (InAs)(GaAs)/GaAsSb quantum well structures as the light-receiving layers. It also describes the low dark currents which were successfully decreased by adding a barrier layer.

Keywords: SWIR sensor, digital alloy, quantum efficiency, barrier layer, dark current

1. Introduction

Short wavelength infrared (SWIR) sensors are used in a variety of fields, including agriculture, environmental monitoring, resource exploration, biomedical diagnostics, and remote sensing. Their demand is increasing. The 1.8–2.5 μm wavelength range is particularly important for identifying substances such as plastics, glucose, and proteins, requiring sensors that operate over a wide wavelength range from 1 to 2.5 μm.[1]-[5] Furthermore, because the absorption specific to the substance in the short wavelength infrared region is weak, high sensitivity (high quantum efficiency) and low noise (low dark current) are required for accurate analysis. Sensors with a light-receiving layer made of HgCdTe (MCT) are commonly used in this wavelength range, but they require cooling with liquid nitrogen or a cryocooler to reduce dark current.[6] The addition of a cooling mechanism increases power consumption, size, and cost, hindering the expansion of application fields. Another issue is the presence of RoHS-regulated substances such as Hg and Cd. On the other hand, sensors with lattice-matched InGaAs on an InP substrate as the light-receiving layer have low dark current and do not require a cooling mechanism. They are also used in photodiodes for optical communication, making them highly manufacturable. However, InGaAs lattice-matched to InP has a cutoff wavelength*1 of only 1.7 μm and is not sensitive to wavelengths longer than 1.7 μm. Using lattice-mismatched InGaAs, the cutoff wavelength reaches 2.6 μm, but the dark current increases and a cooling mechanism is required, similar to MCT.[7], [8] We have developed a sensor with the cutoff wavelength of 2.5 μm that can be cooled by a Peltier device using an InGaAs/GaAsSb type II quantum well structure lattice-matched to InP as the light-receiving layer.[9], [10] Type-II quantum well structures utilize the absorption that occurs at the overlap between the wave functions of electrons confined in the InGaAs conduction band and holes confined in the GaAsSb valence band. The magnitude of this wave function overlap is proportional to the quantum efficiency. Here, theoretical calculations have shown that replacing the InGaAs in the quantum well with an InAs/GaAs digital alloy structure increases the wave function overlap and improves quantum efficiency.[11]-[13] In this report, we describe the fabrication and characteristics of a sensor using a (GaAs)(InAs)/GaAsSb digital alloy type-II quantum well structure (digital alloy type-II super lattice) as the light-receiving layer. Furthermore, we report on further dark current reduction by adding a barrier layer.

2. Digital Alloy Type II Quantum Well Structure

Quantum well structures, consisting of alternating semiconductor layers with different bandgaps on the nanometer scale, are classified into distinct types based on their specific band alignment. Under this classification, a structure in which electrons and holes are confined within the same layer is Type I, whereas a structure in which they are confined within different layers is known as Type II. In this Type II configuration, optical transitions occur across the interface of different semiconductor layers; this enables light absorption at energies corresponding to a narrow effective bandgap while it comprises large-bandgap material. Figure 1 shows the structure of one period of a conven-

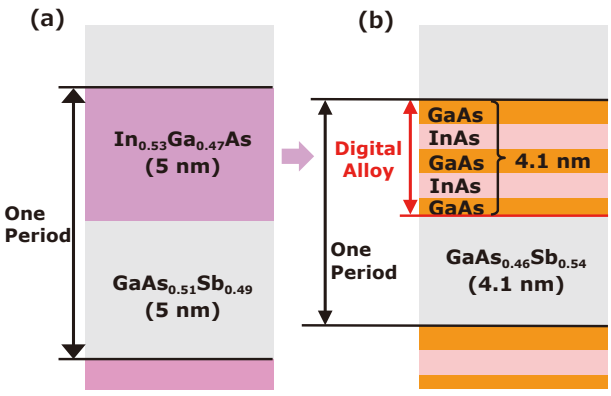

Fig. 1. One period of quantum well (a) C-T2SL, (b) DA-T2SL

tional InGaAs/GaAsSb Type II quantum well structure (called C-T2SL) and the newly developed digital alloy type II quantum well structure (called DA-T2SL). DA-T2SL is composed of $(GaAs)_3/(InAs)_3/(GaAs)_3/(InAs)_3/(GaAs)_2/GaAsSb$. Here, $(GaAs)_3$ represents a GaAs layer with a thickness of three monolayers.

Figure 2 (a) shows the band diagram of the C-T2SL. The absorption occurring at the overlap between the wave functions of electrons confined in InGaAs and holes confined in GaAsSb corresponds to wavelengths of 2 µm range. Figure 2 (b) illustrates the band diagram of the newly developed DA-T2SL. While holes remain confined within the GaAsSb layers as in conventional structures, electrons are distributed throughout the digital alloy layer, maximizing their density near the GaAsSb interface. Consequently, this enhanced overlap at the heterointerface increases absorption, resulting in superior responsivity within the 2 µm spectral region.

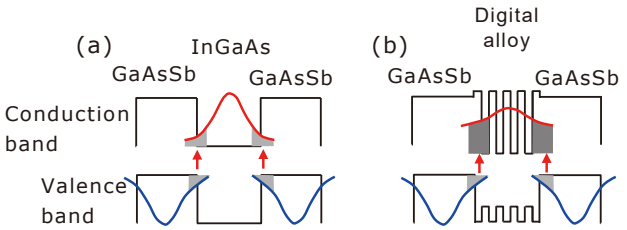

Fig. 2. Band diagrams (a) C-T2SL, (b) DA-T2SL

3. Epitaxial Growth and Sensor Fabrication

3-1 Epitaxial growth

Molecular beam epitaxy (MBE) was used to sequential growth of an n-type InGaAs layer (500 nm thick), an InGaAs layer (50 nm thick), a DA-T2SL light-receiving layer (305 periods), an InGaAs layer (800 nm thick), and a p-type InGaAs contact layer (200 nm thick) on a (001) n-type InP substrate. The crystal quality of the grown DA-T2SL was evaluated using scanning transmission electron microscopy (STEM), high-resolution X-ray diffraction (XRD), and photoluminescence (PL).

In addition, to compare sensor characteristics, epitaxial growth was also performed in which the light-receiving layer was replaced with a C-T2SL (250 periods). The 250 periods were used to match the thickness of the DA-T2SL (305 periods). Furthermore, to confirm the effectiveness of the barrier layer, we also performed epitaxial growth in which the InGaAs layer (50 nm thick) was replaced with an AlGaInAs barrier layer (100 nm thick).

(1) Scanning Transmission Electron Microscopy (STEM)

Figure 3 (a) shows a high-angle annular dark-field (HAADF) image of the DA-T2SL light-receiving layer obtained by STEM. The periodic image contrast closely corresponds to the designed layer thickness, demonstrating that the $(GaAs)_3/(InAs)_3/(GaAs)_3/(InAs)_3/(GaAs)_2$ digital alloy and GaAsSb quantum wells are precisely formed at the atomic scale. Furthermore, the absence of dislocations indicates excellent crystal quality. Figure 3 (b) displays the elemental line scan results obtained by energy-dispersive X-ray spectroscopy (EDX). These results confirm that the layers corresponding to the contrast in the HAADF-STEM image are composed of the elements exactly as designed.

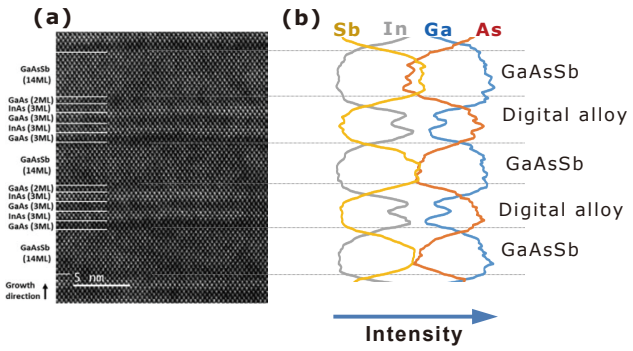

Fig. 3. (a) Cross-sectional HAADF STEM image, (b) EDX line scan of DA-T2SL

(2) X-ray Diffraction (XRD)

Figure 4 shows the X-ray diffraction (XRD) results of a epitaxial wafer with 305-period DA-T2SL light-receiving layer grown for sensor fabrication.

Satellite peaks from −5th to +5th orders corresponding to the repeat period of the $(GaAs)_3/(InAs)_3/(GaAs)_3/(InAs)_3/(GaAs)_2$ digital alloy layer (design thickness 4.1 nm) and the GaAsSb layer (design thickness 4.1 nm) were observed. The difference of angle between each satellite peak corresponds to the thickness of one quantum well period (4.1 nm + 4.1 nm = 8.2 nm), confirming that the digital alloy layer and GaAsSb layer were grown with the designed thickness and sharp interface throughout the 305 periods. Furthermore, the lattice mismatch of the DA-T2SL light-receiving layer, estimated from the difference between the zero-order peak and the peak of the InP substrate, was approximately 0.2%, confirming that there were no lattice mismatch issues.

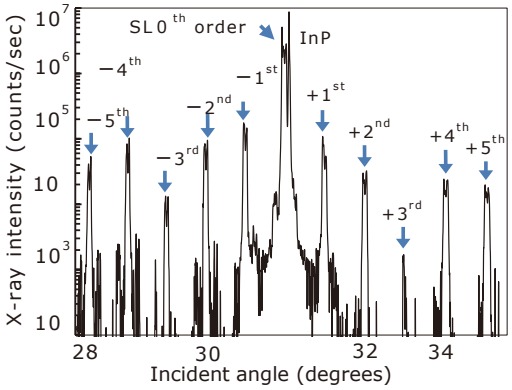

Fig. 4. X-ray diffraction of DA-T2SL epitaxial wafer

(3) Photoluminescence (PL)

Figure 5 shows the temperature dependence of photoluminescence (PL) spectra for the DA-T2SL. Clear PL

emission was observed across the temperature range 200 K to 300 K.

At 250 K, the peak wavelength and full width at half maximum (FWHM) were 2.41 μm and 83 meV, respectively. As the temperature increased from 200 K to 300 K, the peak position exhibited a redshift from 2.37 μm to 2.46 μm.

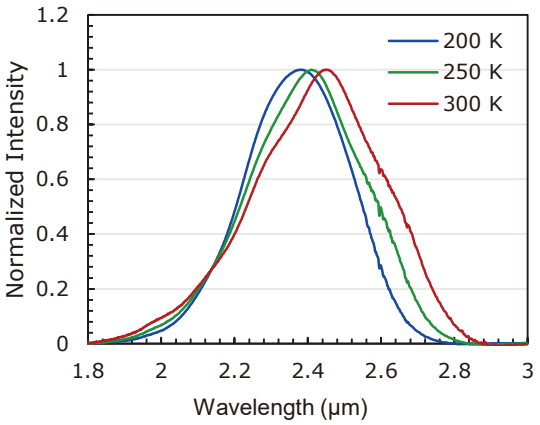

Fig. 5. PL measurement results for DA-T2SL

3-2 Sensor fabrication and evaluation

STEM, XRD, and PL measurements confirmed that the epitaxially grown DA-T2SL structure had good crystal quality, so we proceeded to sensor fabrication. The fabricated sensor structure is shown in Fig. 6. We used both DA-T2SL (305-period) and C-T2SL (250-period) as light-receiving layers. A circular mesa with a diameter of 230 μm was formed on each wafer using a dry etching process.

The surface of the p-type InGaAs contact layer and the mesa sidewalls were then passivated with a SiO_2 film, and ohmic electrodes were formed on the n-type InGaAs buffer layer and p-type InGaAs contact layer. To confirm the effectiveness of the barrier layer, we also fabricated a sensor in which the InGaAs layer directly below the DA-T2SL receiving layer was replaced with an AlGaInAs barrier layer. Finally, the quantum efficiency and dark current of the fabricated sensor were evaluated.

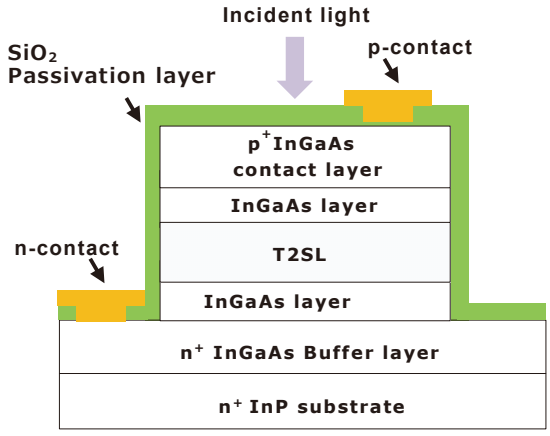

Fig. 6. Schematic cross-section of the sensor (without barrier layer)

(1) Quantum efficiency

Figure 7 shows the external quantum efficiency*2 spectra of sensors using the DA-T2SL and C-T2SL as light-receiving layers. Measurements were performed under top-illumination conditions at 250 K with a bias voltage of −1 V.

The spectral response system used for these measurements consisted of a blackbody radiation source with a mechanical chopper (CL System SR200-33), a monochromator (Acton SP2300), a lock-in amplifier (NF Corporation LI5640), and a liquid nitrogen-cooled Dewar assembly. The cutoff wavelength of the DA-T2SL sensor was 2.5 μm, equivalent to that of the C-T2SL sensor. Furthermore, the DA-T2SL sensor exhibited higher quantum efficiency than the C-T2SL sensor in the wavelength range from 1.8 to 2.5 μm, consistent with theoretical predictions.

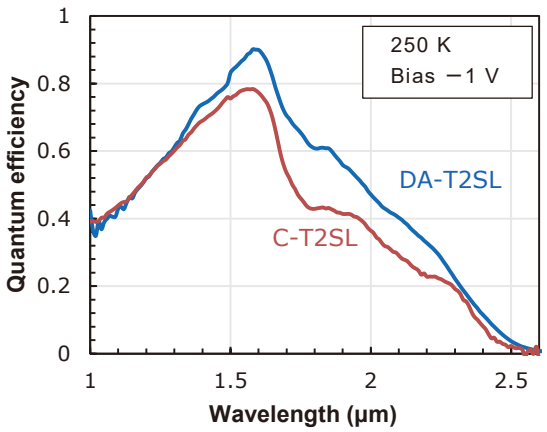

Fig. 7. Comparison of quantum efficiency between DA-T2SL and C-T2SL sensors (250 K, Bias −1 V)

(2) Dark current

Figure 8 shows the dark current characteristics of a sensor using a DA-T2SL light-receiving layer with and without a barrier layer. Because this sensor can be used with zero bias voltage, the bias voltage was set to −100 mV. Adding a barrier layer reduced the dark current by more than one order of magnitude across the entire temperature range from 200 K to 300 K.

Without a barrier layer, the dark current was 1×10^{-6} A/cm^2 at 200 K, while with a barrier layer, it was 1×10^{-6} A/cm^2 at 240 K. While a four-stage Peltier device is required to achieve 200 K, a two-stage Peltier device can achieve 240 K. If the addition of a barrier layer reduces the dark current and allows for the use of Peltier devices with fewer stages, low cost, compact size, and low power consumption are expected.

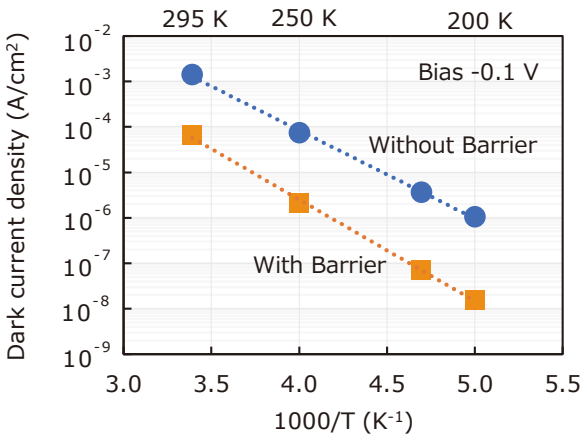

Fig. 8. Dark current comparison of DA-T2SL sensor with and without barrier layer

4. Conclusion

We developed a sensor using an (InAs)(GaAs)/GaAsSb digital alloy type-II quantum well structure as the light-receiving layer. Structural analysis using STEM, XRD, and PL confirmed excellent crystal quality, and we achieved improved quantum efficiency compared to conventional InGaAs/GaAsSb type-II quantum well structures. Furthermore, by inserting an AlGaInAs layer as a hole barrier, we succeeded in reducing dark current by more than one order of magnitude. These characteristics make sensors using an (InAs)(GaAs)/GaAsSb digital alloy type-II quantum well structure as the light-receiving layer promising for a wide wavelength range (1–2.5 μm) and expanding their applications in various fields. We will continue to develop image sensors by fabricating them into 2D arrays.

5. Acknowledgments

This paper is based on results obtained from the project (JPNP22013) commissioned by the New Energy and Industrial Technology Development Organization (NEDO).

Technical Terms

∗1 Cutoff wavelength: The maximum wavelength of light that the sensor can detect.

∗2 External quantum efficiency: The ratio of the number of charge carriers (electrons) actually extracted from the sensor to the number of photons incident on the sensor.

References

(1) T. Kawahara, K. Machinaga, B. Sundararajan, K. Miura, M. Migita, H. Obi, T. Fuyuki, K. Fujii, T. Ishizuka, H. Inada,and Y. Iguchi, “InGaAs/GaAsSb type-II quantum-well focal plane array with cutoff-wavelength of 2.5μm,” Proc. SPIE 10111, 1011115 (2017)

(2) G. A. Tidhar and R. Segal, “New applications with a SWIR imager employing long wavelengths,” Proc. SPIE 8012, 801207 (2011)

(3) L. A. Sordillo, L. Shi, D. C. Sordillo, P. P. Sordillo, and R. R. Alfano, “Advances in medical applications using SWIR light in the wavelength range from 1000 to 2500nm,” Proc. SPIE 10873, 108730T (2019)

(4) J. Roubichou, J. L. Reverchon, A. Evirgen, C. Theveneau, V. Gueriaux, J. L. Gach, and J. L. Beuzit, “Study of new types of detectors in the SWIR (Short Wave InfraRed): Extension of the operating band beyond 1.7μm,” Proc. SPIE 13046, 1304604 (2024)

(5) M. Delmas, D. Ramos, R. Ivanov, L. _Zurauskait, D. Evans, D. Rihtnesberg, S. Almqvist, S. Becanovic, E. Costard,and L. Hoglund, “High performance type- II InAs/GaSb superlattice infrared photodetectors with a short cut-off wavelength,” Opto-Electron. Rev. 31, e144555 (2023)

(6) A. Rogalski, “Infrared detectors for the future,” Acta Phys. Pol., A 116, 389 (2009)

(7) Xiaoli Ji, Baiqing Liu, Hengjing Tang, Xue Li, Ming Shi, Ying Zhou, Yue Xu, Haimei Gong, and Feng Yan, “Improvement of surface leakage current of 2.6μm InGaAs photodetectors by using inductive coupled plasma chemical vapor deposition technology,” Japanese Journal of Applied Physics 54, 04DG09 (2015)

(8) Ying Zhou, Xiaoli Ji, Ming Shi, Hengjing Tang, Xiumei Shao, Xue Li, Haimei Gong, Xun Cao, and Feng Yan, “Impact of SiNx passivation on the surface properties of InGaAs photo-detectors,” J. Appl. Phys. 118, 034507 (2015)

(9) H.Inada, K.Miura, H.Mori, Y.Nagai, Y. Iguchi, and Y. Kawamura, “Uncooled SWIR InGaAs/GaAsSb type II quantum wells focal plane array,” Proc. of SPIE 7660, 76603N-1 (2010)

(10) S. Balasekaran, H. Inada, Y. Iguchi, T. Katsuyama, T. Sasaki, “Photocapacitance characterization of deep levels in InGaAs/GaAsSb type-II MQW photodiodes,” Infrared Physics & Technology, vol. 88, p. 194-199 (2018)

(11) T. Kato and S. Souma, “Optical properties of (GaAs/InAs)–GaAsySb1_y digital alloy superlattices in the short wavelength infrared region calculated by an sp3d5s_ tight-binding method,” Appl. Phys. A 129, 429 (2023)

(12) Takashi Kato, Makoto Murata, Sundararajan Balasekaran, Yasuhiro Iguchi, Yojiro Nakayama, and Satofumi Souma, “(GaAs/InAs)-GaAsSb digital alloy type-II superlattice for extended short-wavelength infrared detection,” Appl. Phys. Lett. 125, 161103 (2024)

(13) Sundararajan Balasekaran, Makoto Murata, Y. Iguchi, “Comparative study of digital and random alloy T2SLs on InP substrates,” Proc. SPIE. 13469 (2025)

Contributors

The lead author is indicated by an asterisk (∗).

B. SUNDARARAJAN*
• Ph.D.
Assistant General Manager, Transmission Devices Laboratory

M. MURATA
• Ph.D.
Transmission Devices Laboratory

Y. IGUCHI
• Ph.D.
Senior Assistant General Manager, Transmission Devices Laboratory